TURBULENT THERMAL INSULATION OF TOROIDAL PLASMAS

R. JONES

Physics Department, Division of Mathematical and Physical Sciences, Emporia State University, Emporia, Kansas 66801, USA.

ABSTRACT

Turbulent thermal insulation can substantially improve the performance of a toroidal plasma confinement device.

THE closed magnetic surfaces of toroidal plasma confinement devices can be destroyed by perturbations such as those due to field errors or magnetic fluctuations[1,2]. Various authors have suggested, for instance, that transport in diffuse toroidal pinches (such as Tokamaks and reverse field pinches) is dominated by magnetic field stochasticity[2–4]. Under such conditions the equation describing radial heat conduction,

$$(dT/dt) = (K_\perp/3nk)\nabla^2 T, \tag{1}$$

is supplemented by the relation

$$K_\perp = K_\parallel (dB/B)^2, \tag{2}$$

where T is the plasma temperature, n the plasma density, B the confining magnetic field, dB the magnetic perturbation field, k the Boltzmann constant, t the time, $K_\perp$ the cross field thermal conductivity, and $K_\parallel$ the thermal conductivity along the (perturbed) magnetic field.

Combining (1) and (2) and simplifying,

$$\frac{T}{\tau_E} = \frac{K_\parallel}{3nk}(dB/B)^2 \frac{2T}{r^2}, \tag{3}$$

where τ_E is the energy confinement time and r the plasma minor radius. Inserting the definition

$$K_\parallel = 3n\lambda^2\nu = (3nv^2/\nu), \tag{4}$$

in (3) we obtain the scaling law for the confinement time

$$\tau_E \approx (r/v_e)^2 (B/dB)^2 \nu, \tag{5}$$

where v_e is the electron thermal speed, λ the electron mean free path length, and ν the electron collision frequency.

This scaling (equation 5) is fatal to many conventional fusion reactor designs. Magnetic field line stochasticity typically arises when $dB/B \geq 10^{-5}$. For a typical RFP reactor design[5] $r \approx 200\,\text{cm}$, $T = 20{,}000\,\text{eV}$, and $n = 3.5 \times 10^{14}\,\text{cm}^{-3}$. For these values and classical Coulomb collisionality

$$\nu = 3 \times 10^{-6} \frac{n \ln(\Lambda)}{T^{3/2}}, \tag{6}$$

equation 5 predicts a confinement time of $\tau_E \sim 10^{-2}\,\text{s}$. The scaling implied by (5) and (6) is

$$\tau \alpha n r^2. \tag{7}$$

Turbulent thermal insulation[6–8] can substantially improve upon this result[9]. In the presence of (ambient or) injected ion acoustic (or other) microturbulence, equation 6 can be replaced by[10]

$$\nu \approx \omega_{pe}(W/nT), \tag{8}$$

where ω_{pe} is the electron plasma frequency and W is the wave energy density. (The presence of *small*

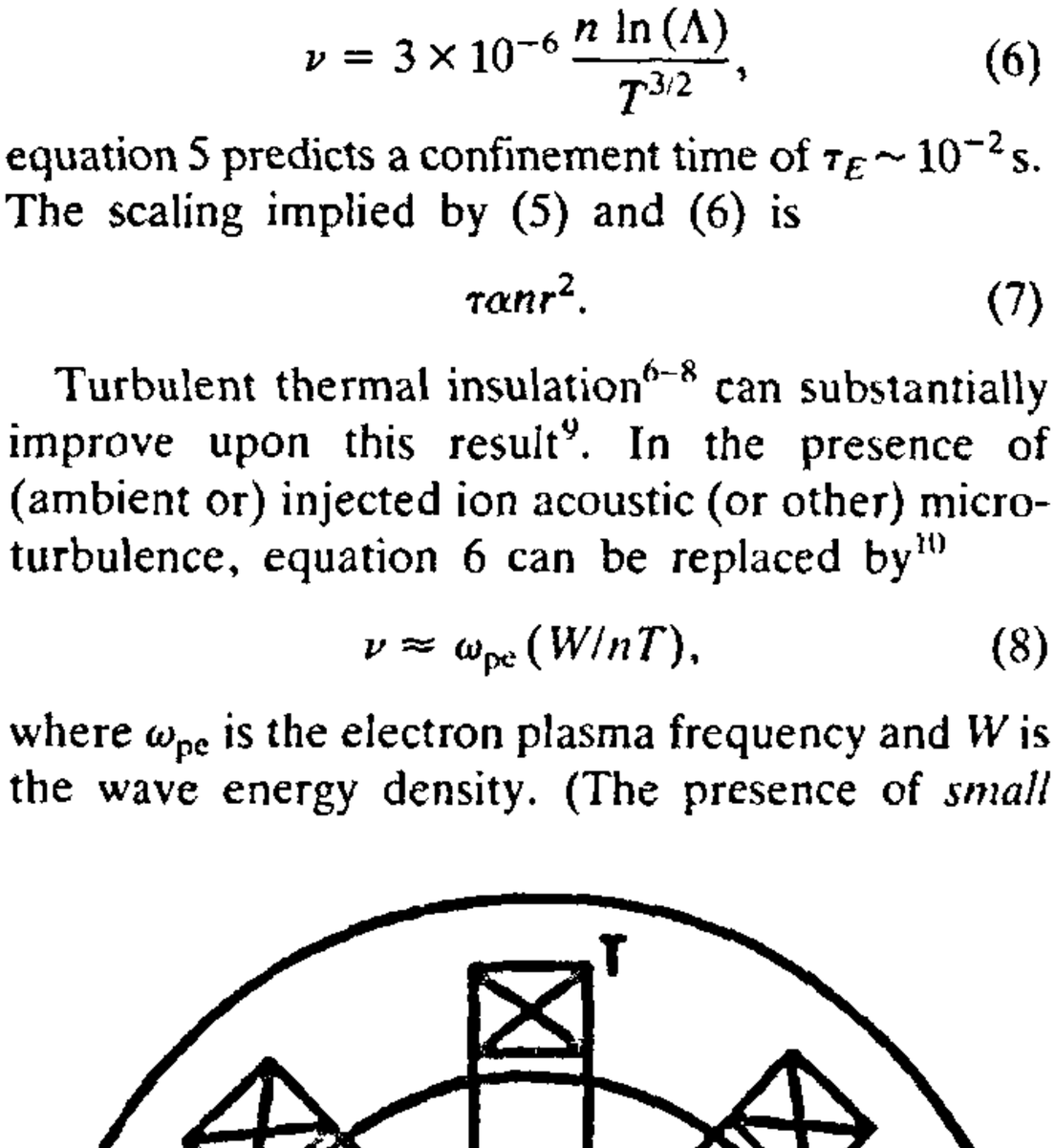

Figure 1. Toroidal plasma device consisting of RF antennae S, toroidal field coils T, vacuum chamber C, plasma column P, and probes L.

Table 1.

RF frequency	:	2.45 GHz
Neutral pressure	:	few × 10^{-4}
Electron temperature	:	5–20 eV
Ion temperature	:	1–10 eV
Plasma density	:	10^9–10^{12} cm^{-3}
Plasma minor radius	:	4–5 cm
Plasma major radius	:	20 cm
Toroidal magnetic fields	:	0–1000 G
Fill gas	:	H_2, He and A

amounts of high Z impurities may also increase the Coulomb collision frequency and result in improved confinement.)

The turbulent insulation effect is limited by the concurrent turbulent heating which will become excessive if the plasma cooling rate does not at least balance the turbulent heating rate, i.e.,

$$\frac{T}{\tau_E} = \frac{W\nu}{n}. \qquad (9)$$

Simultaneous solution of (5), (8) and (9) for the parameters previously cited gives $\tau_E \sim 1$ s which is compatible with typical RFP reactor assumptions[5] and two orders of magnitude improved over the classical Coulomb collision dominated confinement predicted using (5) and (6). The required turbulence level is only $W/nT \approx 10^{-6}$. Similar performance improvements are possible for existing experimental devices.

In order to see how τ scales with reactor size we combine (5), (8) and (9) with the condition that $T =$

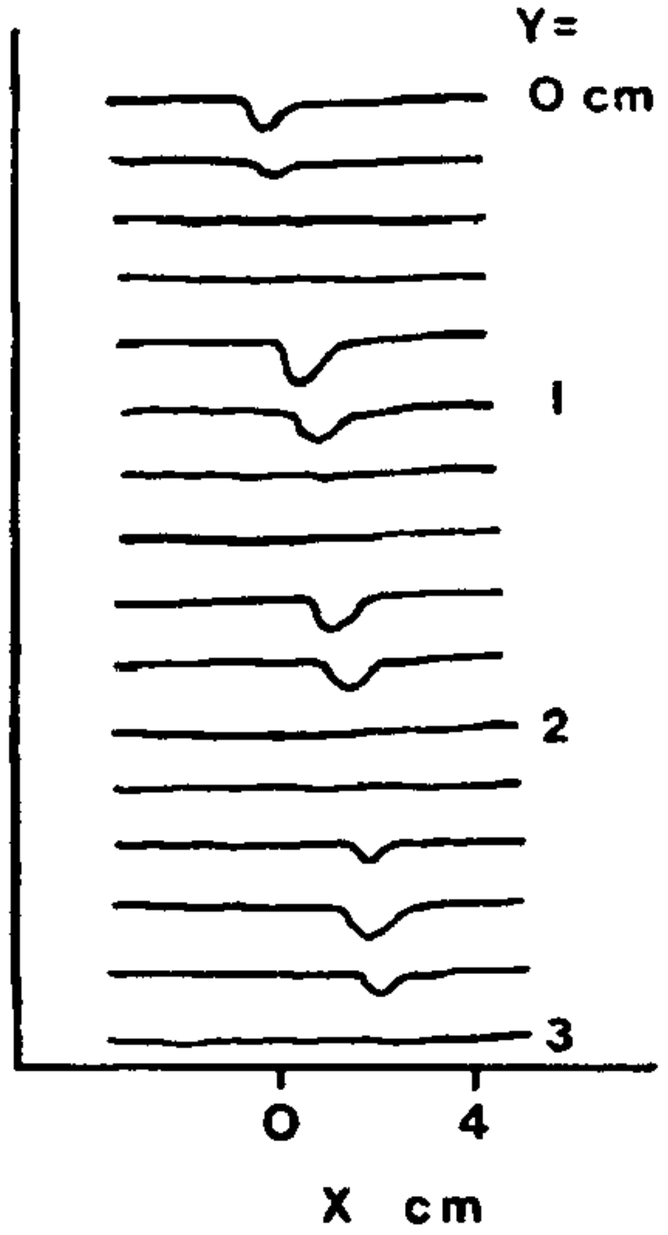

Figure 3. Floating potential profile measured by a Langmuir disc probe scanned across the minor cross-section. The negative dips indicate the location of the electron beam which was injected on

constant to obtain

$$\tau \alpha r^{4/3}. \qquad (10)$$

Magnetic surfaces can be destroyed by field errors as well as magnetic fluctuations[1,11]. The preceding calculations are intended to be rough examples only.

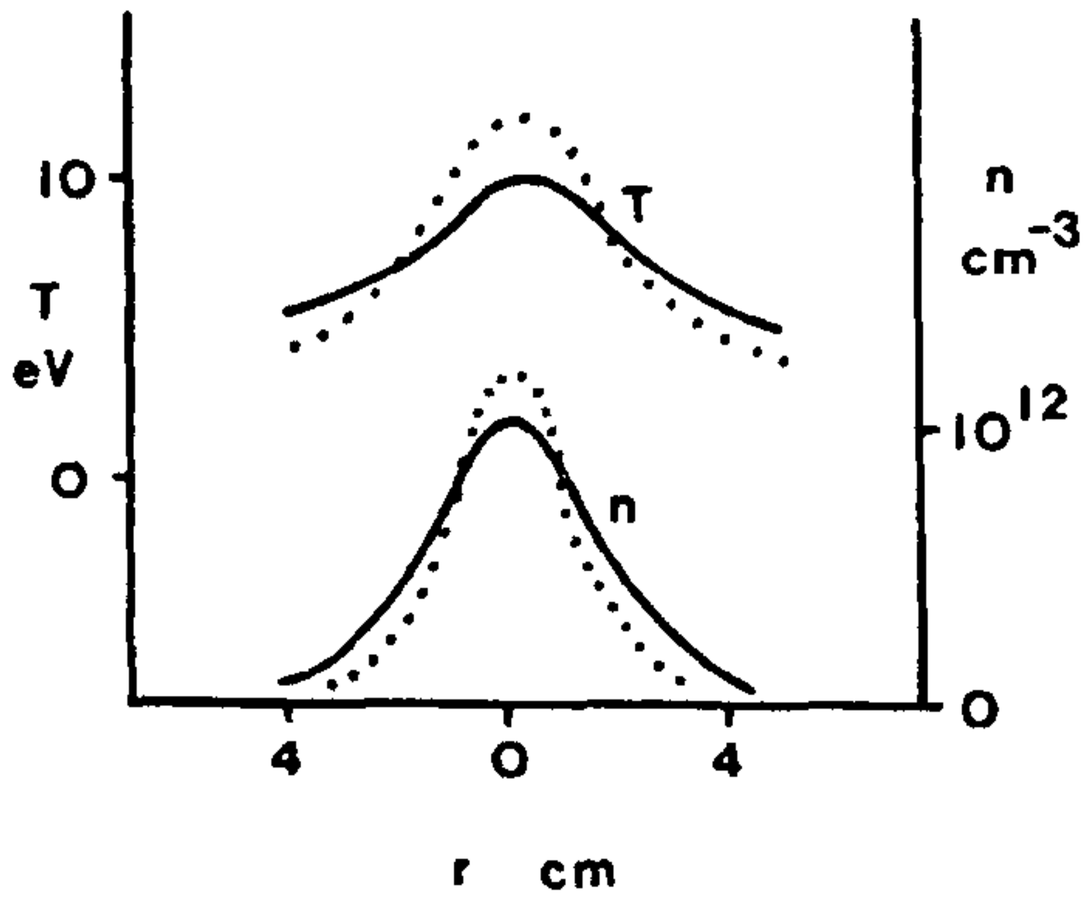

Figure 2. Radial profiles of plasma density, n, and electron temperature T. Dotted curves: with turbulent thermal insulation.

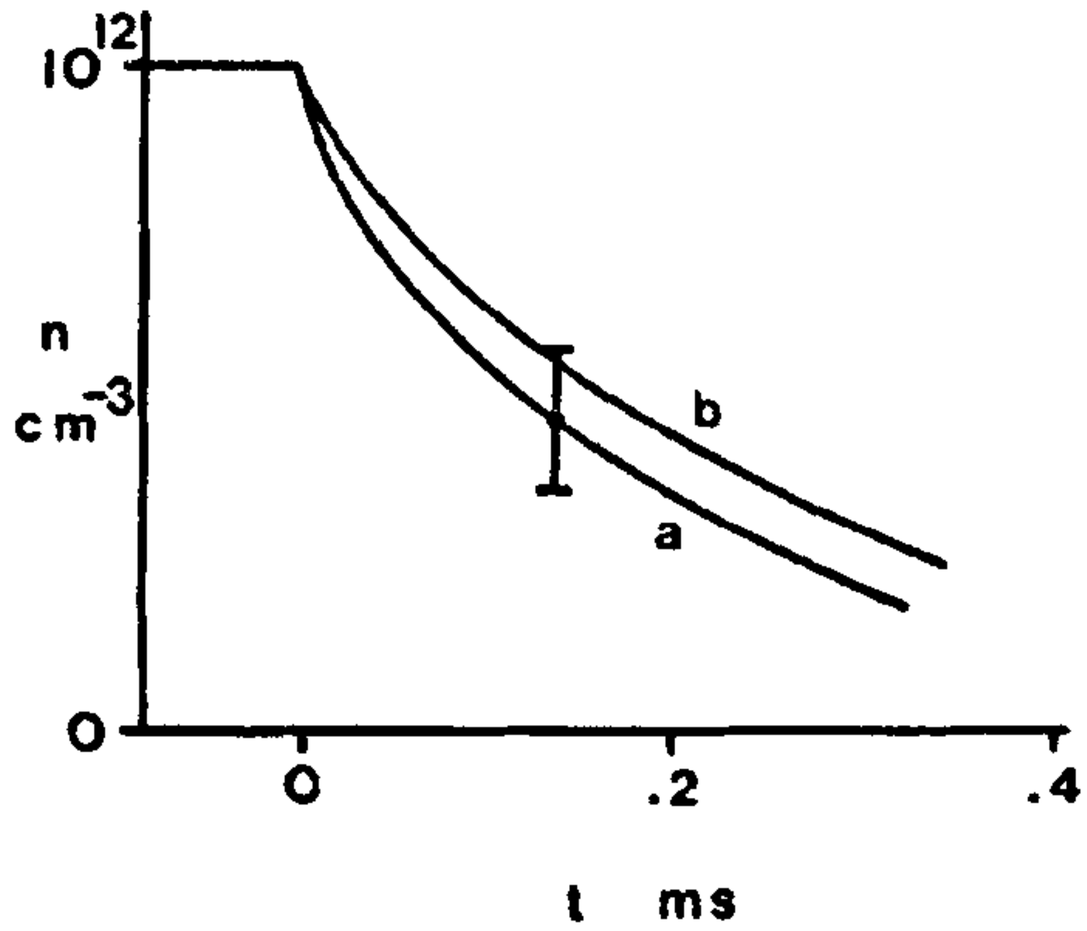

Figure 4. Decay of the plasma in the discharge afterglow. (a) Ion saturation current, and (b) monochrometer signal.

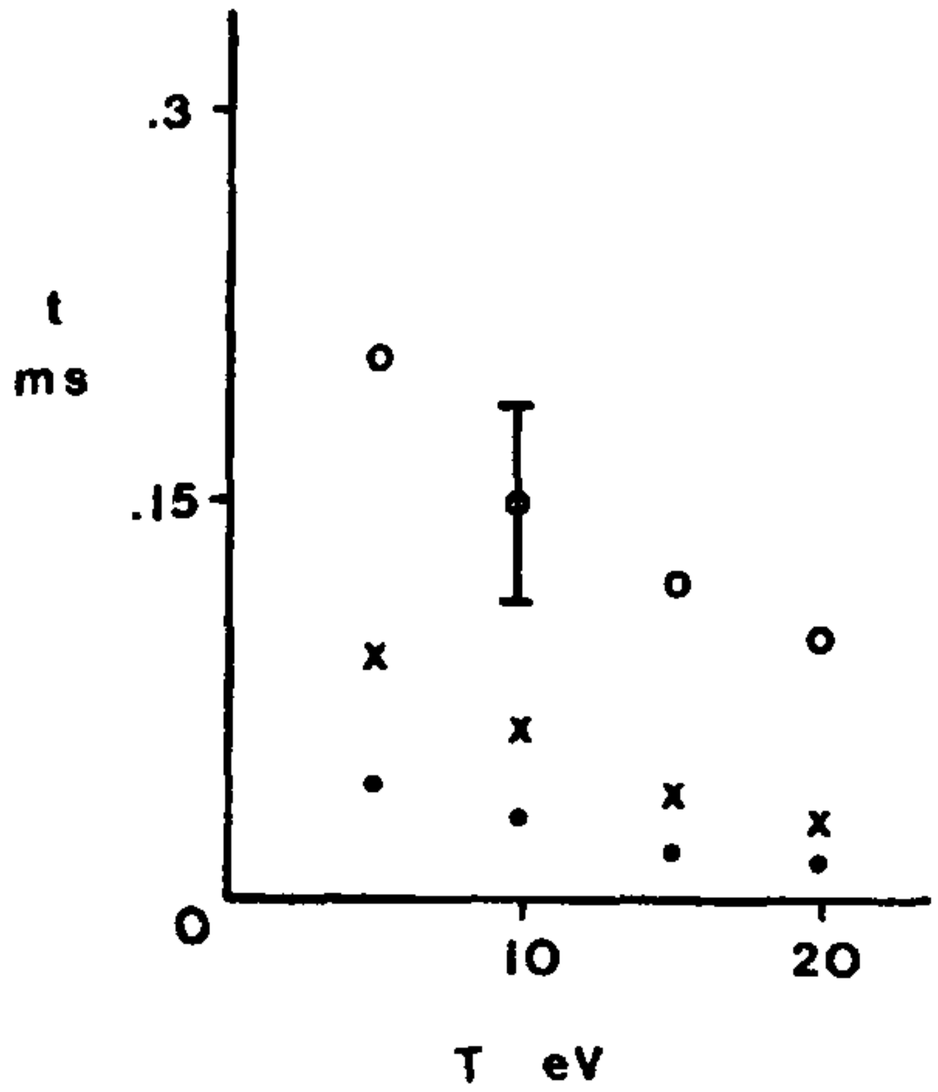

Figure 5. Particle confinement time versus electron temperature. (a) filled circles: hydrogen, (b) crosses: helium, and (c) open circles: argon.

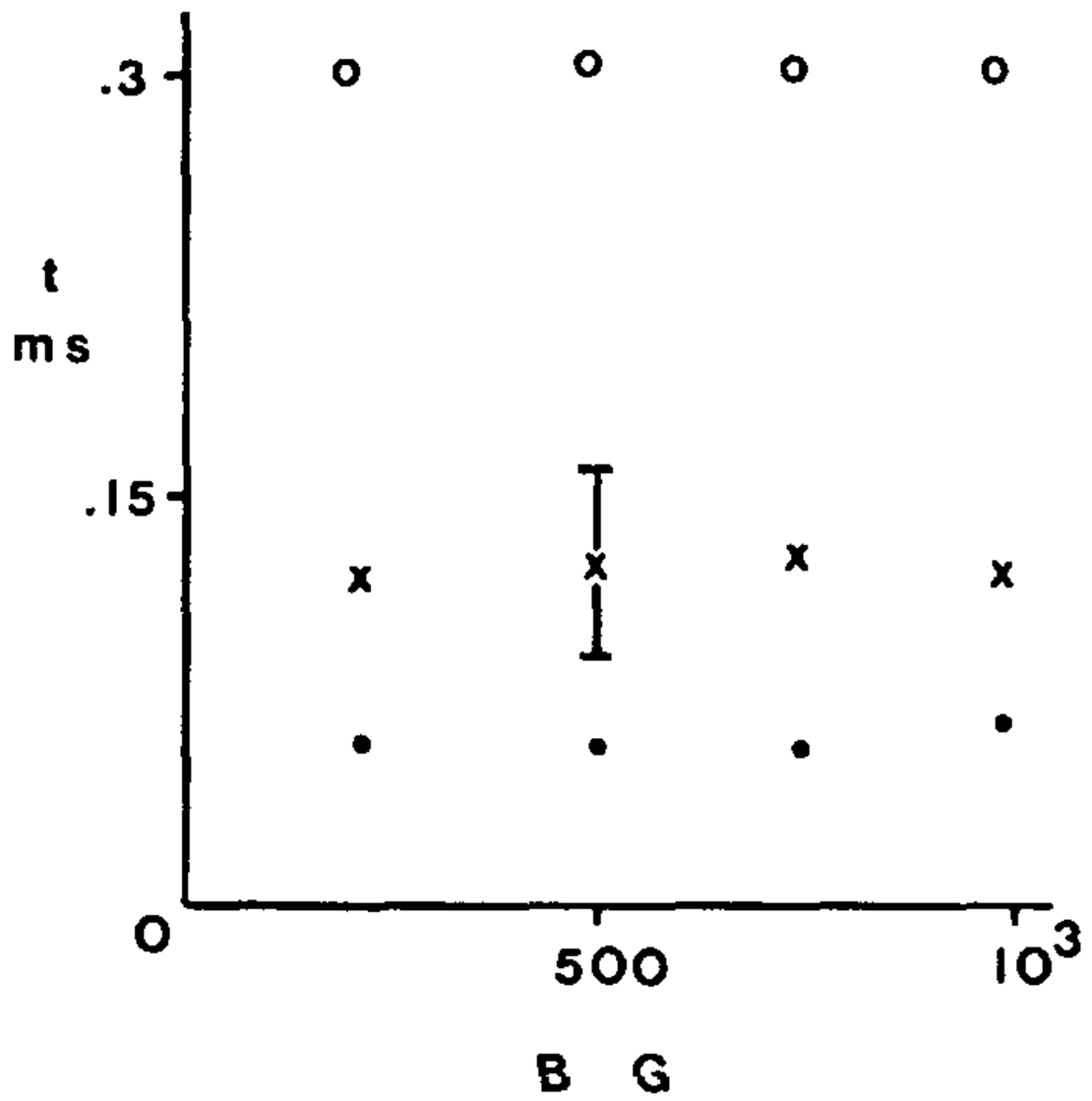

Figure 6. Particle confinement time versus magnetic field. (a) filled circles: hydrogen, (b) crosses: helium, and (c) open circles: argon.

To test these ideas on a small scale the experiments described here were performed in the RSX plasma device illustrated in figure 1. The torus consists of a set of 8 field coils mounted in a circular frame. A rotational transform can be supplied by energizing a stellarator $\ell = 2$ winding (not shown). As in the ACT–1 device at Princeton, equilibria are observed in the absence of magnetic rotational transform[12]. In the experiments described in this paper the helical field windings were not employed. A list of fundamental machine parameters is given in table 1.

An important diagnostic for plasma density and temperature is the Langmuir probe (single, double and triple) scanned in 3 dimensions. Plasma profiles are also measured by spectroscopic means which are non-invasive and hence non-perturbing. An energy analyser is available for ion temperature measurements[13], and calorimeters and thermocouple probes are provided to measure radial particle and heat flux. The diagnostic array has been interfaced to a microprocessor which can document both raw and numerically processed data.

Steady state discharges are sustained by microwave power at a frequency of about 2.54 GHz. Low frequency RF can be coupled to the plasma column through surrounding pairs of copper rings of 4 cm radius. Typical profiles of plasma density and temperature are shown in figure 2.

A tenuous electron beam emitted from a small filament (emissive probe) has been used to map out magnetic field lines. The beam trajectory followed in two dimensions by Langmuir disc probes is helical and indicates the existence of a small (1%) ambient field error (figure 3). This error is presumably due to imperfections in the alignment of the toroidal field coils. Similar results can be observed with the

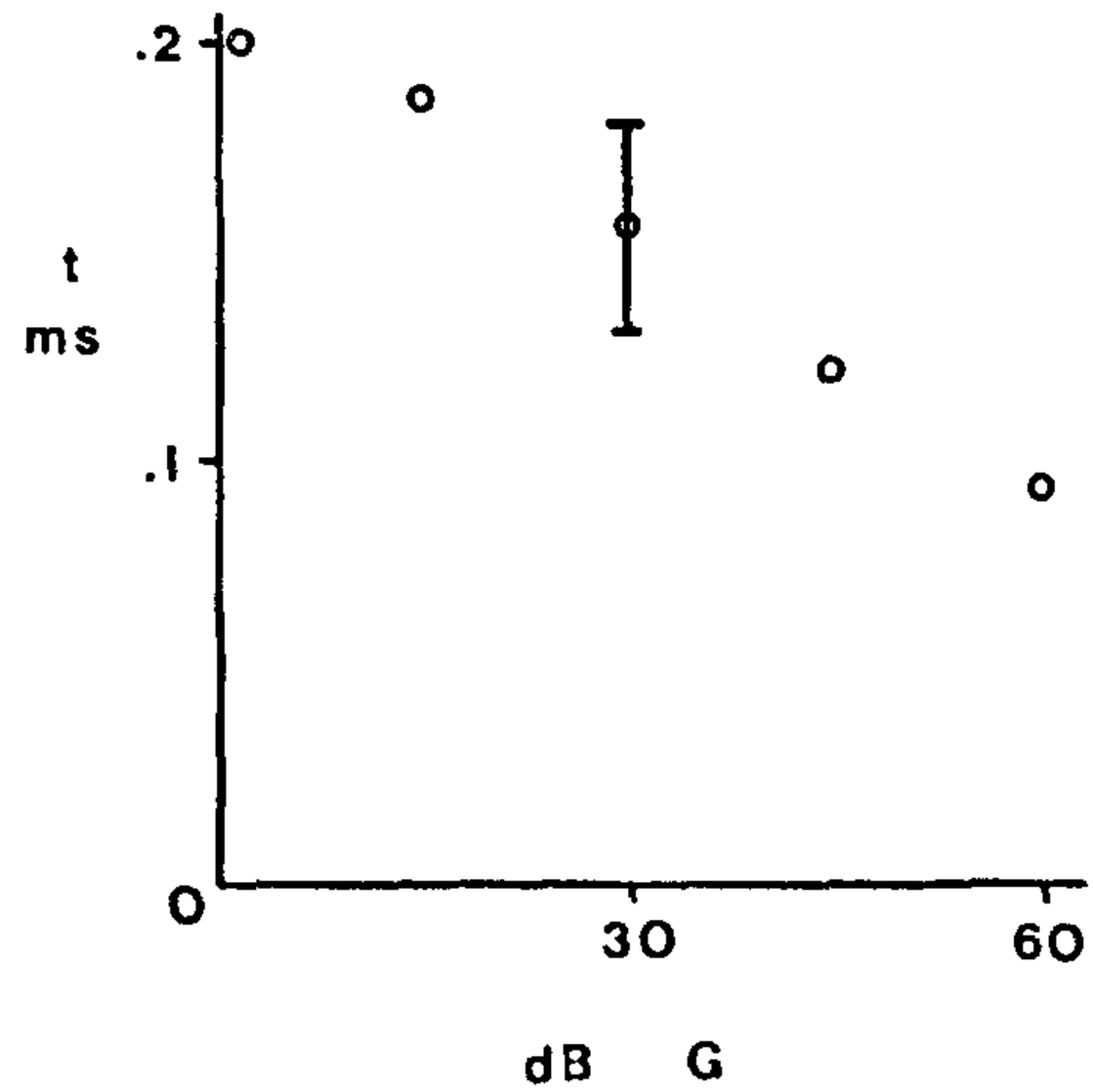

Figure 7. Particle confinement time as a function of dipole field strength measured at the limiter radius.

stellarator windings energized. In either case the device operates as an error field dominated torus.

The variation of plasma density with time in a decaying discharge afterglow is measured by probe ion saturation current and by monochrometer output (figure 4). (The spectroscopic measurements are performed with probes withdrawn and are totally non-perturbing.) The confinement times computed from the slopes are plotted versus plasma electron temperature in figure 5. No variation is seen as a function of toroidal magnetic field over the range of 200 to 1000 G used in the present experiments (figure 6). The functional dependences of the confinement times are consistent with the field error mechanism

$$\tau = C(m_i/kT_e)^{1/2}, \qquad (11)$$

where m_i is the ion mass, T_e the electron temperature and C a constant. The losses can be enhanced by bringing small permanent magnet dipoles near the torus (figure 7).

Under the conditions of the present experiment the mean free path for thermal electron-neutral collisions is typically somewhat less than the distance out of the plasma volume following a perturbed field line.

Having conclusively demonstrated that the plasma losses in our device are attributable to magnetic error fields of order $dB/B \geq 10^{-2}$ we proceeded with an investigation of the effects of the injection of a low level of ion acoustic turbulence. The injected low frequency power was a tiny fraction of the plasma energy and could not directly influence the plasma density and temperature.

In the presence of injected ion acoustic turbulence, $(dn/n)^2 = W/nT \sim 5 \times 10^{-5}$ (as measured by Langmuir probe), the plasma resistivity is observed to increase. The measured resistivity is related to the effective collision frequency through the relation

$$\eta = (m_e\nu/ne^2), \qquad (12)$$

where m_e is the electron mass and e the electronic charge. The resistivity is measured with a probe described in previous publications[7,14].

As the ion acoustic turbulence is turned up the plasma resistivity increases (figure 8), the plasma profiles steepen (figure 2, dotted curves), and the plasma energy density rises.

We have estimated the plasma electron energy confinement time by square wave modulation of the microwave power which sustains the discharge. In figure 9 the electron temperature decay measured by triple probe methods is shown. Curve *a* was taken with a 50% modulation of the microwave power and without turbulent thermal insulation. Curve *b* was taken with 50% microwave modulation and with injected low frequency turbulence $(dn/n)^2$ at a level of about 3×10^{-5}. dn/n was obtained from Langmuir probe data. Curve *c* was taken with 50% microwave modulation and with low frequency injection $(dn/n)^2$ at a level of about 10^{-4}.

Since the ion acoustic turbulence which was injected is of too low a level to directly heat and

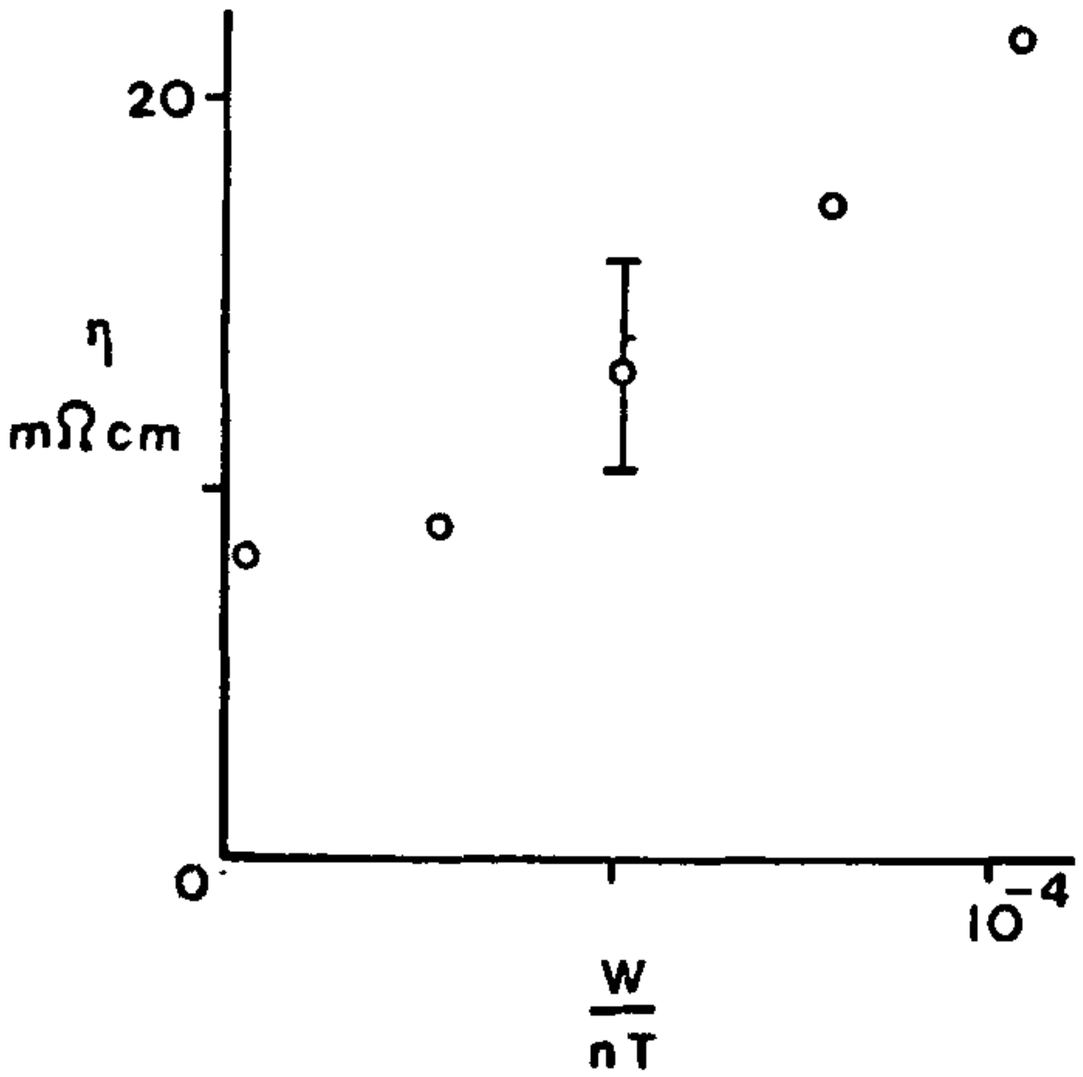

Figure 8. Plasma resistivity as a function of injected ion acoustic turbulence, $f_{ion} = 200$ MHz.

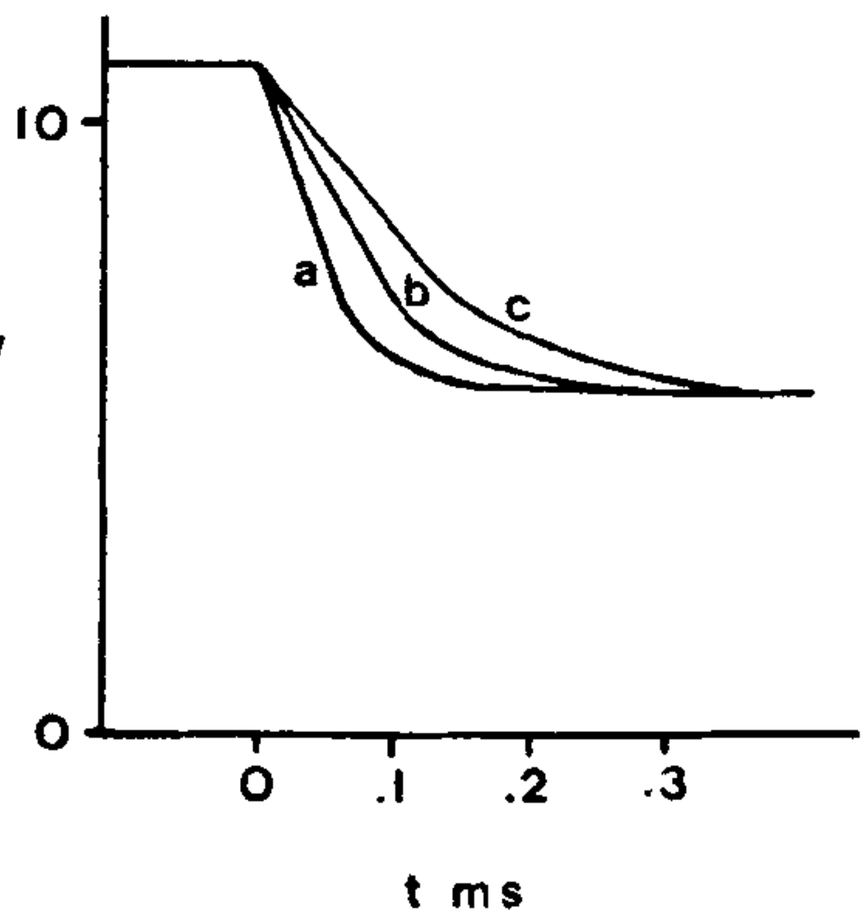

Figure 9. Electron temperature decay measured after the microwave power is decreased by 50% in less than one microsecond.

sustain the plasma (equation 9) we conclude that the enhanced resistivity and confinement time must be attributed to turbulent thermal insulation. We have repeated these experiments in a stellarator configuration (with helical windings energized). So long as the electron beam probing indicates the dominance of the field error loss channel we obtain results which are similar to those seen in figures 5–9.

4 February 1988

1. Kerst, D. W., *Plasma Phys.*, 1962, **4,** 253.
2. Rochester, A. B. and Rosenbluth, M. N., *Phys. Rev. Lett.*, 1978, **40,** 38.
3. Haas, F. A., Thyagaraja, A. and Cook, I., *Plasma Phys.*, 1981, **23,** 1027.
4. Jacobsen, A. R. and Moses, R. W., *Phys. Rev. Lett.*, 1984, **52,** 2041.
5. Bodin, H. A. B., James, T. E., Newton, A. A. and Rostagin, G., In: *Fusion reactor design problems*, Nuclear Fusion Supplement, IAEA, Vienna, 1974, p. 83.
6. Jones, R., *Nuovo Cimento*, 1977, **B40,** 182.
7. Jones, R., *Plasma Phys.*, 1980, **22,** 753.
8. Jones, R., *Plasma Phys.*, 1982, **24,** 445.
9. Jones, R., *Nuovo Cimento*, 1985, **44,** 109.
10. Stenzel, R. L. and Gekelman, W., *Phys. Fluids*, 1978, **21,** 2028.
11. Jernigan, T. C., Prater, R. and Meade, D. W., *Phys. Fluids*, 1971, **14,** 1235.
12. Wong, K. L., Ono, M. and Wurden, G. A., *Rev. Sci. Instrum.*, 1982, **53,** 409.
13. Jones, R., *Rev. Sci. Instrum.*, 1978, **49,** 21; and 1979, **50,** 392.
14. Jones, R., *IEEE Trans. Plasma Sci.*, 1980, **8,** 14.

NEWS

37TH SESSION OF UNITED NATIONS SCIENTIFIC COMMITTEE ON THE EFFECTS OF ATOMIC RADIATION (UNSCEAR)

The United Nations Scientific Committee on the Effects of Atomic Radiation (UNSCEAR) has concluded its 37th session in Vienna and will now submit its final report to the United Nations General Assembly in October. The UNSCEAR session was convened from 6 to 17 June 1988. As in previous years, the Committee's final comprehensive report will be issued as a United Nations sales publication; it will include several annexes containing data and scientific discussions forming the basis of conclusions. UNSCEAR has prepared similar reports since 1958; the latest published edition was in 1986. The 1988 report will include assessment of exposures resulting from the nuclear plant accident at Chernobyl in the USSR on 26 April 1986. Other annexes will cover exposures from natural sources of radiation; exposures from nuclear power production; exposures from medical uses of radiation; genetic hazards; radiation carcinogenesis in humans; and effects on humans of high doses of radiation. — Further information may be obtained from UNSCEAR, A-1400 Vienna, Austria.

(*IAEA Newsbriefs*, Vol. 3, No. 6 (27) July–August 1988, p. 3; published by The Division of Public Information, IAEA, P.O. Box 100, 1400 Vienna, Austria).